Inorg. Chem. **2007**, *46*, 10990–10995

Octacyanotungstate(V)-Based Magnetic Complex Consisting of Dimeric Mn_2 and Tetrameric Mn_2W_2

Zhao-Xi Wang,[†] Xi-Li Li,[†] Tian-Wei Wang,[†] Yi-Zhi Li,[†] Shin-ichi Ohkoshi,[‡] Kazuhito Hashimoto,*[,‡] You Song,*[,†] and Xiao-Zeng You[†]

State Key Laboratory of Coordination Chemistry, School of Chemistry and Chemical Engineering, Nanjing University, Nanjing 210093, China, and Department of Applied Chemistry, School of Engineering, The University of Tokyo, 7-3-1 Hongo, Bunkyo-ku, Tokyo 113-865, Japan

Received February 1, 2007

A novel zero-dimensional (0D) octacyanotungstate(V)–manganese(II) bimetallic assembly, $\{[Mn^{II}(bipy)_2]_2(ox)\}\cdot\{[Mn^{II}(bipy)_2W(CN)_8]_2\}\cdot 4H_2O$ (**1**) (bipy = 2,2′-bipyridine, ox = $C_2O_4^{2-}$), was synthesized in methanol solution containing oxalic acid. X-ray analysis shows **1** is crystallized in monoclinic crystal system with *C*2/*c* space group and composed of two components of a dimeric Mn_2 cation and a quadrate tetrameric Mn_2W_2 anion. The Mn_2 and Mn_2W_2 moieties are connected by their respective π–π stacking to yield the alternative 2D layers, and the 2D layers are linked by hydrogen bonding to form a 3D network. The investigation of the magnetostructural correlation reveals that cyanide and oxalate bridges mediate weak intracluster antiferromagnetic coupling between Mn and W ions and between Mn ions, respectively. Further magnetic measurements and analysis show the spin glasses and intercluster ferromagnetic interaction exist in complex **1**.

Introduction

As zero-dimensional (0D) magnetic materials (magnetic analogues of quantum dots) with potential application in conductors, many clusters showed slow magnetic relaxation behavior when the intermolecule interaction is negligible comparing with intramolecule interaction, which were called single-molecule magnets (SMMs).[1] Similarly, chains can also be considered as one-dimensional (1D) magnetic materials, as suggested by Glauber,[2] i.e., single-chain magnets (SCMs), which have been a hot topic in the field of material science in recent years.[3] In the design and synthesis, Gatteschi raised the point of view that the ratio of the intramolecule interaction and intermolecule interaction must be larger than 10^4 on the basis of Glauber theory for obtaining the low-dimensional magnetic materials. Conversely, when the intermolecule interaction is relatively strong, the magnetic behavior of the low-dimensional magnets disappears. So, the intermolecule magnetic interaction is of great importance, especially to the magnetic properties of a complex with low-dimensional structure. In fact, there have been some reported clusters or chains showing three-dimensional (3D) magnetic properties.[4] However, most of these complexes in the literature did not exhibit pure 3D long-range ordering, due to the presence of spin glasses. As we know, disorder of site or bond in structure and frustration of the magnetic interactions are the two most important prerequisites of spin glass in 3D magnetic complexes. For a lower dimensional complex of cluster or chain, this disorder and frustration were not observed in the spin-glass complexes in the literature.[4] To survey the correlation of spin-glass behavior and inter-

* To whom correspondence should be addressed. E-mail: yousong@nju.edu.cn (Y.S.), hashimoto@light.t.u-tokyo.ac.jp (K.H.).
[†] Nanjing University.
[‡] The University of Tokyo.

(1) (a) Gatteschi, D.; Sessoli, R. *Angew. Chem., Int. Ed.* **2003**, *42*, 268−297. (b) *Magnetism: Molecules to Materials*; Miller, J. S., Drillon, M., Eds.; Wiley-VCH: Weinheim, 2001−2004; Vols. 1−4.
(2) Glauber, R. J. *J. Math. Phys.* **1963**, *4*, 294−307.
(3) (a) Caneschi, A.; Gatteschi, D.; Lalioti, N.; Sangregorio, C.; Sessoli, R.; Venturi, G.; Vindigni, A.; Rettori, A.; Pini, M. G.; Novak, M. A. *Angew. Chem., Int. Ed.* **2001**, *40*, 1760−1763. (b) Clérac, R.; Miyasaka, H.; Yamashita, M.; Coulon, C. *J. Am. Chem. Soc.* **2002**, *124*, 12837−12844. (c) Liu, T.-F.; Fu, D.; Gao, S.; Zhang, Y.-Z.; Sun, H.-L.; Su, G.; Liu, Y.-J. *J. Am. Chem. Soc.* **2003**, *125*, 13976−13977. (d) Wang, S.; Zuo, J.-L.; Gao, S.; Song, Y.; Zhou, H.-C.; Zhang, Y.-Z.; You, X.-Z. *J. Am. Chem. Soc.* **2004**, *126*, 8900−8902. (e) Bai, Y.-L.; Tao, J.; Wernsdorfer, W.; Sato, O.; Huang, R.-B.; Zheng, L.-S. *J. Am. Chem. Soc.* **2006**, *128*, 16428−16429.
(4) (a) Li, D.-F.; Zheng, L.-M.; Zhang, Y.-Z.; Huang, J.; Gao, S.; Tang, W.-X. *Inorg. Chem.* **2003**, *42*, 6123−6129. (b) Kim, J.; Han, S.; Pokhodnya, K. I.; Migliori, J. M.; Miller, J. S. *Inorg. Chem.* **2005**, *44*, 6983−6988. (c) Liu, W.; Wang, C.-F.; Li, Y.-Z.; Zuo, J.-L.; You, X.-Z. *Inorg. Chem.* **2006**, *45*, 10058−10065. (d) Liu, X.-T.; Wang, X.-Y.; Zhang, W.-X.; Cui, P.; Gao, S. *Adv. Mater.* **2006**, *18*, 2852−2856.

10.1021/ic070195c CCC: $37.00
Published on Web 12/01/2007

molecule interaction, we have focused our attention on the synthesis and magnetic properties of octacyanometalate-based low-dimensional complexes $M'[M^{IV/V}(CN)_8]^{4-/3-}$ (M = Mo, W; M′ = transition metal ions), where 2,2-bipyridine (bipy) was introduced as the second ligand to possibly cause the intermolecule magnetic interaction. To keep the stability of $[M^{V}(CN)_8]^{3-}$, acidic reacting medium is necessary, and some small anions were added in the synthesis to balance the oxidation states of M′ metal ions.[5] Some high oxidation states of metal ions such as Mn^{III} ion could also be applied for preventing the reduction of $[M^{V}(CN)_8]^{3-}$. Following this strategy, a novel 0D octacyanotungstate(V)−manganese(II) bimetallic assembly consisting of a pair of ionic species, $\{[Mn^{II}(bipy)_2]_2(ox)\}\cdot\{[Mn^{II}(bipy)_2W(CN)_8]_2\}\cdot 4H_2O$ (**1**; ox = oxalate), was prepared in oxalic acid solution, where Mn^{III} ion was reduced into Mn^{II} ion rather than $[W^{V}(CN)_8]^{3-}$. Herein, we report the details of the synthesis and crystal structure of **1**. Magnetic investigation shows the spin-glass behavior with intercluster ferromagnetic interaction in **1**.

Experimental Section

Syntheses. All chemicals were used as purchased without purification. $Na_3[W(CN)_8]\cdot 4H_2O$ was prepared according to the literature method.[6]

$\{[Mn^{II}(bipy)_2]_2(ox)\}\cdot\{[Mn^{II}(bipy)_2W(CN)_8]_2\}\cdot 4H_2O$. A solution of $Na_3[W(CN)_8]\cdot 4H_2O$ (14.1 mg, 0.026 mmol) in 5 mL of methanol was added to a solution of $MnAc_3\cdot 2H_2O$ (16.4 mg, 0.06 mmol) in 5 mL of methanol, followed by the addition of 6 mL of methanolic solution of oxalic acid (3.2 mg, 0.025 mmol) and bipy (31.2 mg, 0.20 mmol), resulting in a brown-yellow solution mixture. The mixture was placed in the dark, and brown crystals of **1** were obtained after 1 month, in a yield of 78.66%. Anal. Calcd (%) for $C_{98}H_{72}Mn_4N_{32}O_8W_2$: C, 48.77; H, 3.01; N, 18.57. Found: C, 48.52; H, 2.95; N, 18.49. Selected IR data (KBr, cm^{-1}): 2130 (ν_{-CN}), 2161 ($\nu_{\mu-CN}$), 1642 (ν_{-ox}), 1597($\nu_{\mu-ox}$).

Physical Measurements. Elemental analyses for carbon, hydrogen, and nitrogen were carried out with a Perkin-Elmer 240C elemental analyzer. IR spectra were recorded on a Brucker VECTOR22 FT-IR spectrometer using a KBr pellet technique. Variable-temperature magnetic susceptibility measurements on a crystalline sample of **1** were taken at an applied field of 2 kOe on a Quantum Design MPMS SQUID magnetometer working in the temperature range of 300−1.8 K. The molar magnetic susceptibilities are corrected for the diamagnetism estimated from Pascal's tables and for sample holder by previous calibration.

Crystal Structure Determination. Crystal data and details on the data collection and refinement are summarized in Table 1. The crystal data for complex **1** were collected using a Bruker SMART CCD-based diffractometer operating at room temperature. Intensities were collected with graphite-monochromatized Mo Kα radiation (λ = 0.710 73 Å) operating at 50 kV and 30 mA, using the ϕ and ω scan technique. The data reduction was made with the Bruker SAINT package. Absorption corrections were performed using the SADABS program. The structures were solved by direct methods and refined on F^2 by full-matrix least-squares using SHELXL-2000 with anisotropic displacement parameters for all non-hydrogen atoms. Hydrogen atoms were introduced in calculations using the riding model. All computations were carried out using the SHELXTL-2000 program package.[7]

Table 1. Crystallographic Data for **1**

empirical formula	$C_{98}H_{72}Mn_4N_{32}O_8W_2$
formula weight	2413.34
crystal system	monoclinic
space group	*C*2/*c*
a (Å)	43.846(9)
b (Å)	15.669(3)
c (Å)	16.258(3)
β (deg)	97.38(3)
V (Å^3)	11077(4)
Z	4
ρ_{calcd} (g/cm^3)	1.447
μ (mm^{-1})	2.576
GOF (F^2)	1.075
R1[a]	0.0565
wR2[b] [$I > 2\sigma(I)$]	0.1226

[a] $R1 = \Sigma||F_o| - |F_c||/\Sigma|F_o|$. [b] $wR2 = [\Sigma w(|F_o^2| - |F_c^2|)^2/\Sigma w(|F_o^2|)^2]^{1/2}$.

Results and Discussion

Crystal Structure. X-ray crystallgraphy reveals that **1** contains two parts, the dimeric cation $\{[Mn^{II}(bipy)_2]_2(ox)\}$ (Mn_2) and the tetrameric anion $\{[Mn^{II}(bipy)_2W^{V}(CN)_8]_2\}$ (Mn_2W_2), where the oxidation states of each manganese ion was determined to be +2 by the bond valence calculation method proposed by Liu.[8] A view of the dinuclear portion with atom labeling is illustrated in Figure 1a, which is composed of two $Mn^{II}(bipy)_2$ units bridged by a bidentate oxalate dianion. Two bipy ligands and two oxygen atoms of the bridging oxalate are bound to each Mn(II) center of the dinuclear cation, with each metal center having a distorted octahedral geometry. The Mn−O bond lenghths range from 2.186(4) to 2.200(4) Å, and the Mn−N bonds are from 2.029(6) to 2.260(5) Å (Table 2). The Mn2···Mn3 distance is 5.670 Å, which is identical to those reported.[9] Oxalate dianion is approximately planar (mean deviation from the oxalate plane is 0.0081 Å), and the two Mn atoms lie on the plane with the deviations of 0.0000 Å for Mn2 and −0.0001 Å for Mn3 from the plane, respectively. The C−O bond lengths of 1.210(7) and 1.225(7) Å are shorter than the value of around 1.25 Å normally observed for bidentate coordination of oxalate ion.[9] The C−C bond of 1.557(12) Å is comparable with those found in literatures[9] but slightly shorter than 1.574(2) Å in uncoordinated oxalate ion.[10]

The structure of the Mn_2W_2 part shown in Figure 1b consists of double $[W^{V}(CN)_8]^{3-}$ and $[Mn(bipy)_2]^{2+}$ moieties which are built from a square linked by cyano bridges. $W^{V}(CN)_8$ takes a strongly distorted dodecahedron geometry, in which two cyanides (C1N1 and C5N5) connect to the two neighboring $[Mn(bipy)_2]^{2+}$ units, while the other cyanides

(5) Song, Y.; Ohkoshi, S.; Arimoto, Y.; Seino, H.; Mizobe, Y.; Hashimoto, K. *Inorg. Chem.* **2003**, *42*, 1848−1856.
(6) Pribush, R. A.; Archer, R. D. *Inorg. Chem.* **1974**, *13*, 2556−2563.
(7) SMART, SAINT, SADABS, and SHELXTL, Bruker AXS Inc., Madison, WI, 2000.
(8) Liu, W.; Thorp, H. H. *Inorg. Chem.* **1993**, *32*, 4102−4105.
(9) (a) Deguenon, D.; Bernardinelli, G.; Tuchagues, J. P.; Castan, P. *Inorg. Chem.* **1990**, *29*, 3031−3037. (b) Glerup, J.; Goodson, P. A.; Hodgson, D. J.; Michelsen, K. *Inorg. Chem.* **1995**, *34*, 6255−6264. (c) García-Couceiro, U.; Castillo, O.; Luque, A.; García-Terán, J. P.; Beobide, G.; Román, P. *Cryst. Growth Des.* **2006**, *6*, 1839−1847.
(10) Hodgson, D. J.; Ibers, J. A. *Acta Crysrallogr. Sect. B* **1969**, *25*, 469−477.

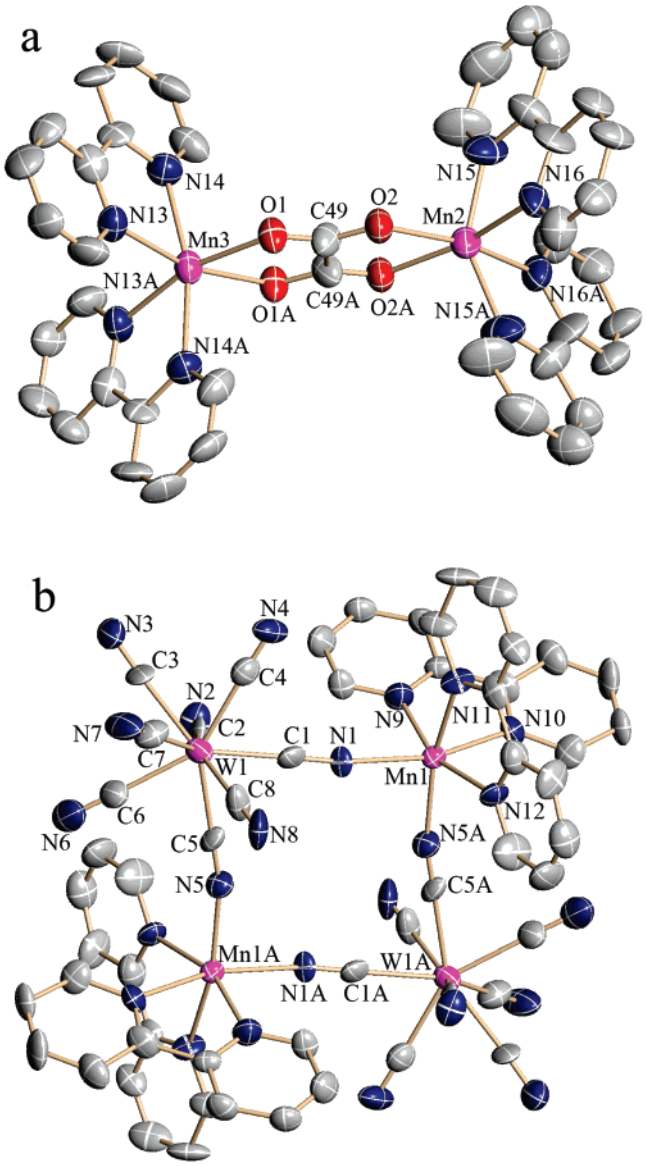

Figure 1. View of the cation (a) and anion (b) showing ellipsoids at the 50% probability level. Hydrogen atoms have been omitted for clarity. (symmetrical code: a, $-x + 1$, y, $-z + {}^1/_2$; b, $-x + {}^1/_2$, $-y + {}^3/_2$, $-z + 2$).

are terminal. The mean W−C and C−N distances are 2.141 and 1.131 Å, respectively, and the W−C−N units are almost linear from 177.3(5)° to 179.0(6)°, but the W−C−N−Mn linkages are poorly linear, with torsion angles of 152.0° and −99.0°. The Mn atoms are also six-coordinate, showing a distorted octahedral geometry with six N atoms from two bipy and two cyano bridges, respectively. The bond lengths of Mn1−N range from 2.167(5) to 2.288(4) Å, which are identical to those observed in Mn(II) complexes.

In the solid state, the Mn_2 and Mn_2W_2 moieties extend to a two-dimension network in the *bc* plane, respectively, by the collective interaction of $\pi-\pi$ stacking of the bipy rings and hydrogen bonding, which is shown in Figure 2. The arm-to-arm $\pi-\pi$ stacking of the bipy rings connects the Mn_2 clusters to form the Mn_2-based cation layers with pyridyl centric distances of 3.573 and 4.022 Å along the two diagonal directions of the *b* and *c* axes, while the face-to-face $\pi-\pi$ interaction connects Mn_2W_2 clusters, resulting in anion layers

Table 2. Selected Bond Distances (Å) and Bond Angles (deg) for **1**

C1−N1	1.151(6)	W1−C1	2.140(6)
C2−N2	1.130(6)	W1−C2	2.153(6)
C3−N3	1.125(6)	W1−C3	2.141(5)
C4−N4	1.115(6)	W1−C4	2.162(6)
C5−N5	1.127(5)	W1−C5	2.172(5)
C6−N6	1.123(6)	W1−C6	2.134(6)
C7−N7	1.159(7)	W1−C7	2.139(7)
C8−N8	1.097(6)	W1−C8	2.151(6)
Mn1−N1	2.245(4)	Mn2−N15	2.029(6)
Mn1−N5[a]	2.167(5)	Mn2−N16	2.260(5)
Mn1−N9	2.222(5)	Mn2−O2	2.200(4)
Mn1−N10	2.256(4)	Mn3−O1	2.186(4)
Mn1−N11	2.288(4)	Mn3−N13	2.240(5)
Mn1−N12	2.254(4)	Mn3−N14	2.219(5)
C49−O2	1.210(7)	C49−C49[b]	1.557(12)
C49−O1	1.225(7)		
W1−C1−N1	179.0(4)	Mn1−N1−C1	169.2(3)
W1−C2−N2	177.9(4)	Mn1−N5−C5[a]	167.4(4)
W1−C3−N3	177.3(5)	N1−Mn1−N5[a]	94.74(17)
W1−C4−N4	178.2(5)	N1−Mn1−N9	90.84(16)
W1−C5−N5	178.5(4)	N1−Mn1−N10	162.33(16)
W1−C6−N6	178.4(6)	N1−Mn1−N11	88.41(16)
W1−C7−N7	177.7(5)	N1−Mn1−N12	102.52(16)
W1−C8−N8	179.0(6)	N5−Mn1−N10[a]	91.47(17)
N15−Mn2−O2	101.0(2)	N5−Mn1−N11[a]	163.66(18)
N15−Mn2−O2[b]	105.6(2)	N5−Mn1−N12[a]	92.94(17)
N15−Mn2−N16	74.2(2)	N9−Mn1−N10	71.75(17)
N15−Mn2−N16[b]	84.8(3)	N9−Mn1−N11	95.75(18)
N16−Mn2−N16[b]	101.7(3)	N10−Mn1−N11	90.27(17)
O2−Mn2−O2[b]	73.6(2)	N10−Mn1−N12	93.65(17)
O1−Mn3−O1[b]	75.10(19)	N11−Mn1−N12	70.73(17)
O1−Mn3−N13	95.36(16)	N13−Mn3−N13[b]	96.2(3)
O1−Mn3−N13[b]	164.89(17)	N13−Mn3−N14[b]	96.04(19)
O1−Mn3−N14	96.47(18)	N13−Mn3−N14	73.92(19)
O1−Mn3−N14[b]	95.23(18)	N14−Mn3−N14[b]	165.2(3)

[a] Symmetry transformation used to generate equivalent atoms: $-x + {}^1/_2$, $-y + {}^3/_2$, $-z + 2$. [b] Symmetry transformation used to generate equivalent atoms: $-x + 1$, y, $-z + {}^1/_2$.

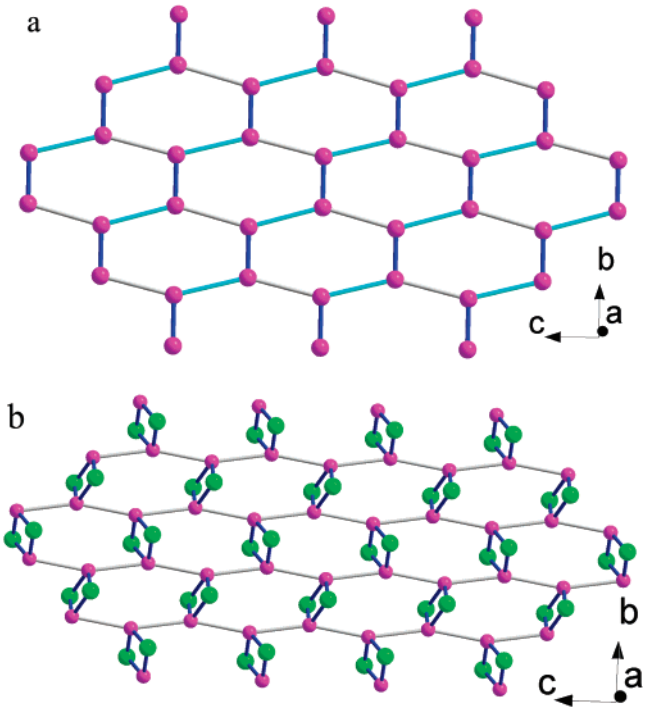

Figure 2. Projection of the cation (a) and anion (b) networks formed by the metal atoms in the *bc* plane. (Sphere colors: green, W; pink, Mn. Line colors: blue, oxalate or cyanide bridging; gray and cyan, $\pi-\pi$ interaction).

with a pyridyl distance of 4.689 Å. The cation and anion layers arrange alternatively. Uncoordinated water molecules

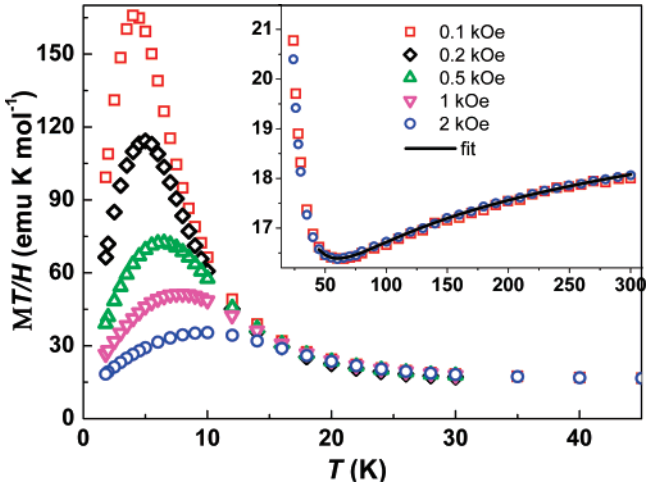

Figure 3. Magnetic susceptibilities of **1** at various fields. Fitting results: $g = 1.98(1)$, $J = -10.2(4)$ cm^{-1}, $J' = -2.5(1)$ cm^{-1}, TIP $= 1.5(3) \times 10^{-3}$ emu mol^{-1}, and $zj' = 0.38(3)$ cm^{-1} with $R = 1.8 \times 10^{-4}$.

are occupied in the spacing of the two neighboring layers, and there are two kinds of hydrogen bonds in the structure. The lattice water molecules are linked by O3−H3B···O4, O4−H4A···O6 (symmetrical code x, y, $z + 1$), O5−H5B···O7, and O6−H6B···O8 hydrogen bonds. Simultaneously, these water molecules interact with N atoms of $[W(CN)_8]$ by O6−H6···N4 (symmetrical code x, $y - 1$, $z - 1$), O5−H5A···N6 (symmetrical code x, y, $z - 1$), O7−H7A···N2 (symmetrical code x, $-y + 1$, $z - {}^1/_2$), and O4−H4B···N7 (symmetrical code x, $-y + 1$, $z - {}^1/_2$) hydrogen bonds. These hydrogen bonds further connect the cation and anion layers to form a 3D network.

Magnetic Properties. Magnetic susceptibility measurements of the crystalline sample of **1** were carried out at various fields, as shown in Figure 3, and two regions are clearly distinguished. In the high-temperature region (above ~45 K), the $\chi_M T$ lines superimpose, but at low temperatures, $\chi_M T$ strongly depends on the applied fields, which is also observed in another octacyanotungstate−manganese complex.[11] As a typical measurement under an applied field of 0.1 kOe, the room-temperature $\chi_M T$ value is 18.0 emu K mol^{-1}, slightly lower than the spin-only value of 18.25 emu K mol^{-1} based on the sum of Mn_2 and Mn_2W_2 ($S = {}^5/_2$ for Mn^{II} and $S = {}^1/_2$ for W^V assuming $g_{average} = 2$). When the system is cooled, the $\chi_M T$ value gradually decreases, reaching a minimum of 16.6 emu K mol^{-1} at 60 K. Below this temperature, $\chi_M T$ goes through a maximum of 166 emu K mol^{-1} around 6 K and then quickly decreases until 1.8 K. This magnetic behavior is quite similar to the ferrimagnetic properties, but the structure of **1** implies that the magnetic properties may be very complicated, which depend on the intracluster coupling interaction. Complex **1** contains Mn_2 and Mn_2W_2 moieties in one unit, in which oxalate always mediates the antiferromagnetic coupling interaction between Mn^{II} ions according to the reported works.[9] Thus, the spin ground state only depends on the tetranuclear Mn_2W_2. Antiferromagnetic or ferromagnetic coupling between Mn and W ions will lead to a spin ground state of $S_T = 4$ or 6 and the corresponding $\chi_M T$ value of 10 or 21 emu K mol^{-1}, respectively. However, the maximum $\chi_M T$ at 0.1 kOe is 166 emu K mol^{-1}, which is much higher than the expected value in either antiferromagnetic or ferromagnetic coupling between Mn and W ions. It is suggested that the long-range ferromagnetic interaction, such as the ferromagnetic coupling between the ground state spins of Mn_2W_2 clusters, does exist in this complex, which may be mediated by the intralayer $\pi-\pi$ staking interaction and the interlayer hydrogen bonding according to the structure shown in Figure S1 (Supporting Information). However, the long-range magnetic interaction does not cause the long-range magnetic ordering above 1.8 K. The evidence is from the zero-field-cooling (zfc) and field-cooled (fc) magnetization measurements shown in Figure 4, in which no bifurcation was observed. The low-field susceptibilities show the strong field dependence in low-temperature region (Figure 3 and Figure S2, Supporting Information). When the applied fields increase, $\chi_M T$ and χ_M quickly go down and the peak of $\chi_M T$ shifts to higher temperature. The peak shift may result from the superparamagnetic behavior of the Mn_2W_2 cluster, which is very similar to the field dependence of the maximum ac susceptibility observed in some low-dimensional magnets.[12] The magnetic data can be simulated by the isotropic spin Hamiltonian $\mathbf{H} = -2J(\mathbf{S}_{Mn1}\mathbf{S}_{W1} + \mathbf{S}_{Mn1}\mathbf{S}_{W1A} + \mathbf{S}_{Mn1}\mathbf{S}_{W1} + \mathbf{S}_{Mn1A}\mathbf{S}_{W1A}) - 2J'\mathbf{S}_{Mn2}\mathbf{S}_{Mn3}$, where J and J' are the coupling constants mediated by cyanide in the Mn_2W_2 cluster and by oxalate in dimer Mn_2, respectively. The expression is written as follows when TIP and the mean-field corrections zj' were taken into account:

$$\chi = \frac{2Ng^2\beta^2}{kT}\left(\frac{A}{B} + \frac{C}{D}\right) + \text{TIP}$$

$$\chi_M = \frac{\chi}{1 - (2zj'/Ng^2\beta^2)\chi}$$

$$A = 106 + 105e^{-2x} + e^{-6x} + 5e^{-x} + 14e^{-10x} + 30e^{-12x} + 5e^{2x} + 14e^{4x} + 30e^{6x} + 55e^{8x} + 91e^{10x}$$

$$B = 39 + 35e^{-2x} + e^{-4x} + 3e^{-6x} + 5e^{-8x} + 7e^{-10x} + 9e^{-12x} + 5e^{2x} + 7e^{4x} + 9e^{6x} + 11e^{8x} + 13e^{10x}$$

$$C = e^{2y} + 5e^{6y} + 14e^{12y} + 30e^{20y} + 55e^{30y}$$

$$D = 1 + 3e^{2y} + 5e^{6y} + 7e^{12y} + 9e^{20y} + 11e^{30y}$$

where $x = J/kT$ and $y = J'/kT$. The calculated results in the temperature range from 45 to 300 K (below 45 K, $\chi_M T$ cannot be fitted due to its dependence on the applied fields) give $g = 1.98(1)$, $J = -10.2(4)$ cm^{-1}, $J' = -2.5(1)$ cm^{-1}, TIP $= 1.5(3) \times 10^{-3}$ emu mol^{-1}, and $zj' = 0.38(3)$ cm^{-1} with $R = \Sigma[(\chi_M T)_{calc} - (\chi_M T)_{obs}]^2/\Sigma(\chi_M T)_{obs}^2 = 1.8 \times 10^{-4}$. It indicates the antiferromagnetic coupling between metal ions mediated

(11) Freedman, D. E.; Bennett, M. V.; Long, J. R. *Dalton Trans.* **2006**, 2829−2834.

(12) (a) Schelter, E. J.; Prosvirin, A. V.; Dunbar, K. R. *J. Am. Chem. Soc.* **2004**, *126*, 15004−15005. (b) Ishikawa, N.; Otsuka, S.; Kaizu, Y. *Angew. Chem., Int. Ed.* **2005**, *44*, 731−733. (c) Lü, Z.; Yuan, M.; Pan, F.; Gao, S.; Zhang, D.; Zhu, D. *Inorg. Chem.* **2006**, *45*, 3538−3548. (d) Wen, H.-R.; Wang, C.-F.; Song, Y.; Gao, S.; Zuo, J.-L.; You, X.-Z. *Inorg. Chem.* **2006**, *45*, 8942−8949.

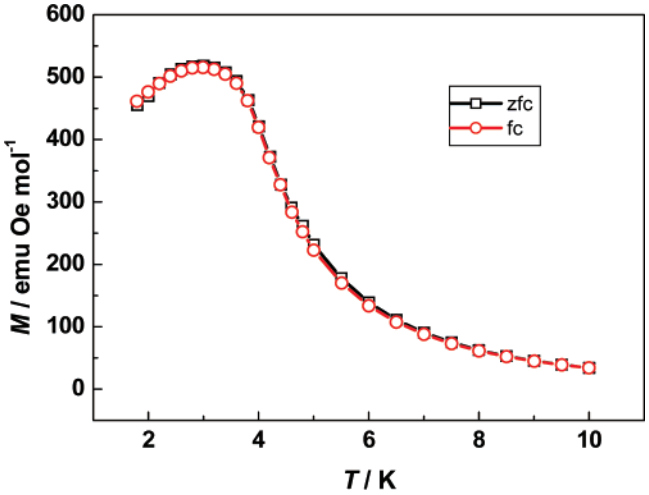

Figure 4. Zero-field-cooling magnetization and field-cooled magnetization plots at an applied field of 10 Oe. The solid lines are for the eyes.

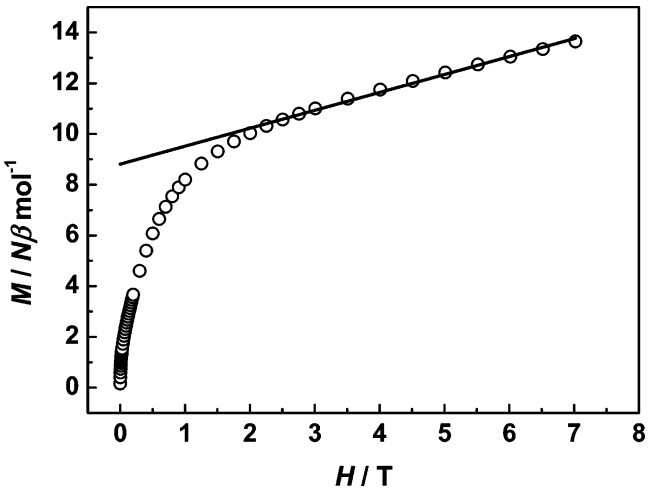

Figure 5. Field dependence of magnetization of complex **1** at 1.8 K.

by bridging ligands of cyanide and oxalate and the weak ferromagnetic interaction between clusters in complex **1**. The value of J' is comparable with those reported previously.[9] Consequently, the ground state spin was determined to be $S_T = 4$ [$=(^5/_2 - {}^1/_2) \times 2 + {}^5/_2 - {}^5/_2$]. In the magnetic measurements of complex **1**, the $M-H$ results in Figure 5 cannot directly give an unambiguous spin ground state but can provide the coupling information between metal ions under fields. Figure 5 can be viewed as two regions, nonlinear and linear ones, respectively, below and above 2 T. The weakly antiferromagnetic coupled Mn_2 dimers have no net magnetization (M_{Mn_2}) due to the net spin of 0. The magnetization of Mn_2 dimers (M_{Mn_2}) will basically display a linear increase with the increasing field because of the decoupling effect of external field on the spins of Mn_2 dimers. Similarly, antiferromagnetic coupled Mn_2W_2 clusters will nonlinearly increase, i.e., quickly increase at low fields and finally reach a saturation state of 8 $N\beta$ mol^{-1} at high fields. Thus, the magnetization of **1** is factually a sum of two contributions from Mn_2 dimers and Mn_2W_2 clusters, $M_{sum} = M_{Mn_2W_2}$ (nonlinear) + M_{Mn_2} (linear). At the linear region above 2 T in Figure 5, it is suggested that the magnetization of Mn_2W_2 clusters reaches saturation, so $M_{sum} = C$ (constant)

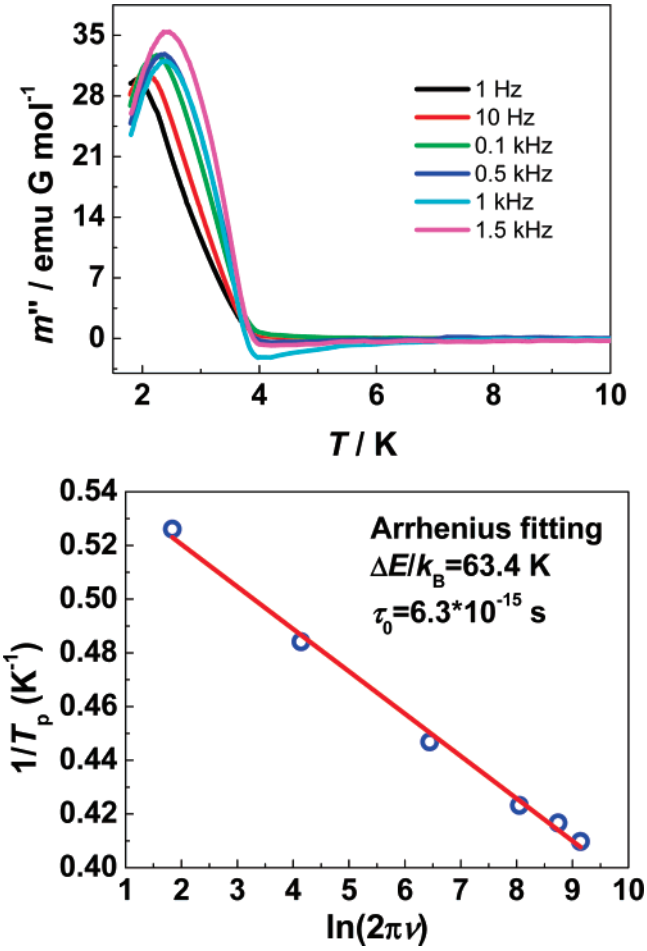

Figure 6. Ac measurements of out-of-phase (top) and Arrhenius fitting (bottom) for complex **1**.

+ M_{Mn_2} (linear). Thus, the constant C was estimated to be 8.8 $N\beta$ mol^{-1} by linear fitting, as shown in Figure 5, which is close to the theoretical value of 8 $N\beta$ mol^{-1} for antiferromagnetic coupled Mn_2W_2 clusters. So, the low-field magnetization of **1** is mainly ascribed to the contribution of Mn_2W_2 clusters. As the field increases, the magnetization of **1** quickly increases and the magnetization of Mn_2W_2 clusters goes to saturation of 8 $N\beta$ mol^{-1} at around 2 T. Above 2 T, the magnetization contribution of Mn_2 dimers leads to a durative linear increase of the magnetization of **1**. This indicates that the field has not been strong enough to cause the spins of Mn_2 to arrange in parallel entirely along the direction of applied field, because the magnetization of **1** (M_{sum}) equals 13.6 $N\beta$ mol^{-1} at 7 T, which is lower than the saturation value of either $M_{Mn_2W_2} + M_{Mn_2} = 8 + 10$ or $12 + 10$ $N\beta$ mol^{-1}.

Ac magnetic measurements of **1** are shown in Figures 6 and S3 (Supporting Information). The obvious frequency dependence of both in- and out-of-phase ac magnetization was observed and the peak temperatures T_p for out-of-phase data fairly obey the Arrhenius law $\tau = 1/2\pi f = \tau_0 \exp(\Delta E/k_B T_p)$ with a linear correlation of $1/T_p$ versus $\ln(2\pi f)$. The fitting results give the relaxation time, $\tau_0 = 6.3 \times 10^{-15}$ s, and the energy barrier, $\Delta E/k_B = 63.4$ K. The very short relaxation time τ_0 suggests spin-glass behavior in **1**. For determining the spin glasses of **1**, two very important

parameters are required. One is the quantitative measurement of the frequency shift ϕ from $(\Delta T_p/T_p)$ per decade ω ($\omega = 2\pi f$). For complex **1**, $\phi = \Delta T_p/[T_p\Delta(\log \omega)] = 0.08$, which is much smaller than that of a superparamagnet mentioned by Mydosh[13] and smaller than the value of 0.1−0.15 found in some low-dimensional magnets.[3c,d,12d] Another quantitative measurement is obtained by fitting the frequency dependence of peak temperature using the conventional critical scaling law of the spin dynamics, $\tau = \tau_0[(T_p - T_f)/T_f]^{-z\nu}$.[14] The fitting results give the parameters $\tau_0 = 2 \times 10^{-5}$ s, $z\nu = 4.83$, and $T_f = 1.6(1)$ K (Figure S4, Supporting Information). The value of $z\nu$ is just in the range of various spin glasses from 4 to 12 and the frozen temperature is 1.6 K.[3c,13] Furthermore, the plots of χ_M' vs frequency at various temperatures give a relatively large fitted α value,[13,15] while no convergent fitting result can be obtained in the plots of χ_M'' vs frequency (Figure S5, Supporting Information). All ac magnetic measurements and deduced results are in agreement with the canonical spin glasses of **1**, which may be ascribed to the long-range ferromagnetic interaction.

As a matter of fact, in those low-dimensional spin-glass complexes, including **1**, randomness and frustration are not observed. Mydosh suggested that intercluster couplings must be added to take into account spin glasses because a spin glass is not a noninteracting collection of clusters.[13] At early time, Mydosh had made some attempts to relate the interaction strengths between the clusters to the origin of a spin glass; however, this assumption was supported by no unambiguous evidence. Besides, there has not been a simple model to approach it to date, because no simple enough examples can give us a feasible idea for modeling. Undoubtedly, complex **1** and the reported works in the literatures may provide some valuable reference on the intermolecule couplings leading to spin-glass behavior. Generally, the low-dimensional complexes with spin-glass behavior all showed the same magnetic characteristics of the short-range magnetic ordering (within cluster or chain) and the long-range disordering with long-range ferromagnetic interaction.[4] The short-range ordering and long-range disordering of spins are just the nature of canonical spin glasses.

In summary, a unique 0D octacyanometalate-based magnetic complex consisting of Mn_2W_2/Mn_2 moieties was synthesized. The short-range ordering within the Mn_2W_2 cluster and the weak long-range ferromagnetic interaction lead to the spin-glass behavior in title compound due to the relatively strong $\pi-\pi$ stacking interaction by the ligand of bipy. This kind of low-dimensional complexes showing spin glasses provides an opening question in magnetism and may be a key for distinguishing spin glasses from low-dimensional magnets (SMMs and SCMs) and pure 3D magnet by intermolecule interaction strengths.

Acknowledgment. This work was supported by the Major State Basic Research Development Program (2006CB806104 and 2007CB925102), National Natural Science Foundation of China (20771057 and 20631030), and Natural Science Foundation of Jiangsu Province (No. BK2006113).

Supporting Information Available: X-ray crystallographic data in CIF format of complex **1**, $\pi-\pi$ stacking diagram, spin dynamics fitting, χ_M' and $\chi_M''-f$ and $M-H/T$ figures. This material is available free of charge via the Internet at http://pubs.acs.org.

IC070195C

(13) Mydosh, J. A. *Spin Glasses: An Experimental Introduction*; Taylor & Francis: London, 1993; pp 64−72.
(14) (a) Zheng, Y.-Z.; Tong, M.-L.; Zhang, W.-X.; Chen, X.-M. *Angew. Chem., Int. Ed.* **2006**, *45*, 6310−6314. (b) Li, X.-J.; Wang, X.-Y.; Gao, S.; Cao, R. *Inorg. Chem.* **2006**, *45*, 1508−1516.
(15) Aubin, S. M. J.; Sun, Z.; Pardi, L.; Krzystek, J.; Folting, K.; Brunel, L.-C.; Rheingold, A. L.; Christou, G.; Hendrickson, D. N. *Inorg. Chem.* **1999**, *38*, 5329−5340.